Polymer Journal, Vol. 39, No. 12, pp. 1312–1318 (2007)

SPECIAL ISSUES -PROGRESS IN STRUCTURE ANALYSES OF POLYMERIC MATERIALS BY SYNCHROTRON RADIATION AND NEUTRON BEAM-

Living Polymerization Induced Macro- and Microdomain Investigated by Focusing Ultra-small-angle Neutron Scattering

Ryuhei MOTOKAWA,[1] You IIDA,[2] Yue ZHAO,[1] Takeji HASHIMOTO,[1] and Satoshi KOIZUMI[1,†]

[1]*Research Group for Soft Matter & Neutron Scattering, Advanced Science Research Center, Japan Atomic Energy Agency, Japan*
[2]*Department of Physics, Tohoku University, Aoba, Aramaki, Aoba-ku, Sendai 980-8578, Japan*

(Received July 12, 2007; Accepted September 28, 2007; Published November 2, 2007)

ABSTRACT: By utilizing a biconcave refractive neutron lens (MgF_2) 5-inch size & high resolution position sensitive area photomultiplier with scintillator (ZnS), we constructed a focusing ultra-small-angle neutron scattering (USANS) spectrometer (SANS-J-II) at research reactor JRR3, Tokai, Japan. SANS-J-II can successfully reach to $q_{min} = 0.0003\,\text{Å}^{-1}$, where $q\ (= 4\pi \sin(\theta)/\lambda)$ is the magnitude of scattering vector given by wavelength λ and scattering angle 2θ, and simultaneously cover conventional small-angle neutron scattering (SANS) region to $q = 0.004\,\text{Å}^{-1}$. Focusing USANS, thus realized, plays an important role to investigate the time-evolution of hierarchically ordered structures in the living radical polymerization solution, preparing poly(methyl methacrylate)-*block*-polystyrene (PMMA-*b*-PS). In the reaction process to synthesize a PS block chain from the end of PMMA block chain, we found the interplay between macro- and microphase separation. SANS at $q > 0.001\,\text{Å}^{-1}$ determined time-evolving microdomain structures; as the polymerization proceeds, (i) first by order-disorder transition, a lamellar microdomain appears and (ii) second by order-order transitions, the morphologies of microdomains change to PMMA cylinder and successively to PMMA sphere. USANS at $q < 0.001\,\text{Å}^{-1}$, exhibiting power law scattering ($\sim q^{-\alpha}$) due to macrophase separation between PMMA-*b*-PS and PS homopolymer (appeared as by product). The exponent α varies from 4 to 2, reflecting a grain boundary of macrodomain rich-in PMMA-*b*-PS; when a lamellar microdomain appears, Porod law gives $\alpha = 4$, whereas when cylinder and sphere appear, $\alpha = 2$, due to inhomogeniety of the microdomain spatial distribution of the microdomains. [doi:10.1295/polymj.PJ2007099]

KEY WORDS Ultra-small-angle Neutron Scattering / Small-angle Neutron Scattering / Living Radical Polymerization / Phase Separation / Microdomain /

In order to address the question of whether small-angle scattering approaches can be used to investigate hierarchically ordered systems in a soft condensed matter, covering length scales ranging from micrometres to angstrom, we have recently developed a focusing neutron ultra-small-angle neutron (USANS) scattering spectrometer (SANS-J-II) at research reactor JRR3, Tokai, Japan.[1] The conventional small-angle neutron scattering (SANS) spectrometer (SANS-J), the q-range of which is limited from $0.003\,\text{Å}^{-1}$ to $0.1\,\text{Å}^{-1}$, was reconstructed by adding advanced neutron optical devices, where $q\ (= 4\pi \sin(\theta)/\lambda)$ is the magnitude of the scattering vector given by the wavelength λ and the scattering angle 2θ. To improve the minimum accessible q_{min} to an order of $0.0001\,\text{Å}^{-1}$, a focusing technique with a biconcave refractive lens made from the compound MgF_2,[2] plays the most important role. Focusing USANS achieved by SANS-J-II is complementary to a Bonse–Hart double-crystal USANS spectrometer, which reaches to $q_{min} = 10^{-5}$ Å^{-1} with grooved perfect crystals and thermal neutrons.[3] Focusing USANS profits to perform time-resolved USANS measurement or to observe highly oriented anisotropic microstructures, which are hardly achieved by a Bonse–Hart spectrometer because of stepwisely scanning of scattering angle or smearing effect by line beam spread.

By employing the focusing USANS technique, we investigated living polymerization solution to prepare diblock copolymer of poly(methyl methacrylate) (PMMA) and polystyrene (PS) (PMMA-*b*-PS) *via* reversible addition–fragmentation chain transfer (RAFT) living radical polymerization.[4,5] In a reaction vessel, we expect that polymerization-induced molecular self-assembly, such as micro- and macrophase separation, occurs when degree of polymerization N or concentration of block copolymer ϕ_P increases during the polymerization and therefore $\phi_P \chi N$ exceeds a critical value for micro- and macrophase separation,[6,7] where χ is the Flory interaction parameter between two different monomers.[8,9] In this paper, we report our recent results of *in situ* and time-resolved focusing

†To whom correspondence should be addressed (Tel: +81-29-284-3511, Fax: +81-29-282-5939, E-mail: koizumi.satoshi@jaea.go.jp).

USANS observations on micro- and macrophase separation induced by living radical polymerization, which is further developed from the results reported elsewhere.[10,11] Focusing USANS has advantages; First, focusing collimation played an important role to determine the morphologies of microdomain structure, the size of which is close to the resolution of conventional pinhole SANS (several hundred angstrom). Secondly, focusing USANS, covering 10^{-4} Å^{-1} order, was able to quantitatively examine macrophase separation.

EXPERIMENT

Materials

Methylmethacrylate (MMA) (Wako Pure Chemical Industries, Ltd., Osaka, Japan) was purified by distillation under vacuum. Styrene-d_8 (Aldrich) was purified with an activated alumina column to remove inhibitor. Initiator, 2,2-azobisisobutyronitrile (AIBN) (Woko Pure Chemical Industries, Ltd., Osaka, Japan), was recrystallized from methanol. Benzene (Aldrich) was distilled in order to use as a solvent. Cumyl dithiobenzoate (CDB: RAFT regent) was synthesized and characterized using the procedure reported in the literature.[12] By using these chemical regents, we synthesized PMMA-*b*-PS *via* RAFT living radical polymerization. This synthesis process is comprised of two reaction processes, *i.e.*, reaction process (I) for PMMA block chain and reaction process (II) for PS block chains from radically activated PMMA block chain end.[11]

Reaction Process (I) (Preparation of PMMA)

First, PMMA having the dithiobenzoate group at the chain end was synthesized and isolated. MMA (84 mmol), CDB (0.05 mmol), and AIBN (0.025 mmol) were dissolved in 3 mL of benzene in a 50-mL round bottom flask. This solution was freeze-thawed three times to remove oxygen. In an oil-bath controlled at 60 °C, living radical polymerization was initiated without stirring. After 24 h of polymerization, the solution was cooled in an ice-bath and the polymerization was stopped. To remove un-reacted MMA, CDB, and AIBN, the polymerization solution was slowly dropped in huge amount of methanol. PMMA, precipitated in methanol, was filtered, and then dried in a vacuum chamber. Thus we obtained PMMA homopolymer, the chain end of which is capped by a dithiobenzoate group, with number-averaged molecular weight $M_n = 121{,}000$ and polydispersity index $M_w/M_n = 1.24$, which were determined by gel permeation chromatography (GPC) measurements calibrated by PMMA standard (Showa Denko) with $M_n = 200$–1500000.

Time-resolved Observation of Reaction Process (II)

PMMA powder of 0.45 g, obtained in reaction process (I), was dissolved in 3.0 g (0.093 mol) of styrene-d_8 in a glass vial tube, then, the mixture was degassed by freeze-thaw method with three times. The prior polymerization mixture of 1.5 mL was poured into a specially designed quartz cell (2 mm thickness) for SANS experiment, which is connected with three-way stopcock and vial glass tube (see Figure 1 in ref. 11). By heating up at 130 °C, reaction process (II) was started. Note that reaction process (II) is bulk polymerization without solvents and radical initiators, where the radicals are generated by self-initiation of styrene monomer.[13] It was clearly observed that at about 100 min after starting reaction process (II), the polymerization solution becomes turbid. This is due to macrophase separation between PMMA-*b*-PS and PS homopolymer (by-product).

The reaction process (II) was monitored by focusing USANS mode (SANS-J-II) and conventional pinhole SANS mode (SANS-J). The scattered neutrons were detected by two-dimensional high-resolution area detector and ^{3}He main detector. The data were corrected for counting efficiency, instrumental background, and air scattering, and then, circular averaging was carried out.

Focusing Ultra-small-angle Neutron Scattering Spectrometer (SANS-J-II)

Focusing USANS spectrometer (SANS-J-II) is installed at the end of a cold neutron guide with a cold neutron flux of 1.0×10^8 (n/cm^2 s) at JRR-3 research reactor (20 MW) at JAEA, Tokai, Japan. Using a disk-type velocity selector[14] provided by Central Research Institute in Hungary, cold neutron is monochromated with the maximum of Maxwellian wavelength distribution at $\lambda = 6.5$ Å with $\Delta\lambda/\lambda = 13\%$. The total spectrometer length (20 m) is symmetrically divided at the sample position; the T-shape collimator and scattering flight tube are about 10 m in length (L_1 and $L_2 \cong 10$ m in Figure 1(a)). The incident beam is narrowly collimated by fourfold beam slits composed of sintereted B_4C plates with a tapered edge and four ultrasonic motors. As shown in Figure 1(a), in the third bank of T-shape collimator, the biconcave refractive lens, made from MgF_2, is installed just before sample position, at a nearly symmetric position (L_1 and $L_2 \cong L_S$), where L_S is distance of sample to detector. We used a focusing lens designed by national insitute of standard and technology (NIST).[2] It is comprised of biconcave MgF_2 crystal (provided by Ohyo Koken Kogyo Co. Ltd, Japan) whose diameter, radius of curvature R, and thickness at center are 30 mm, 25 mm and 1 mm, respectively. We put 70 individual lenses along the beam line to focus neutrons of wave-

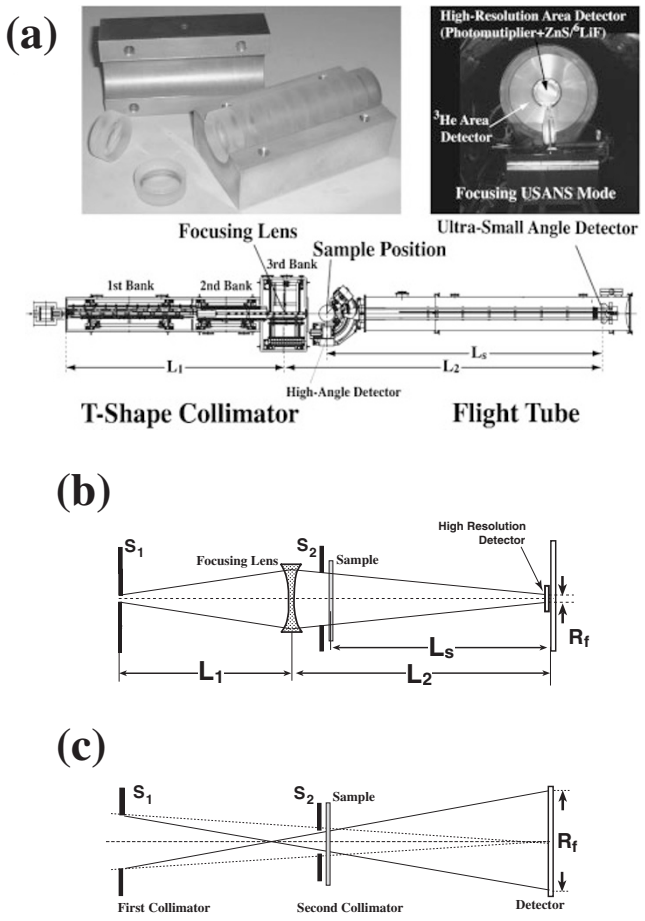

Figure 1. Schematic diagrams of (a) focusing ultra-small angle scattering spectrometer (SANS-J-II) with biconcave refractive lens and high-resolution area detector. By changing pinholes, SANS-J-II is available for (b) focusing USANS with lens, as well as (c) conventional pinhole SANS, where L_1, L_2, and L_3 are distances of first aperture to lens, lens to detector, and sample to detector, respectively.

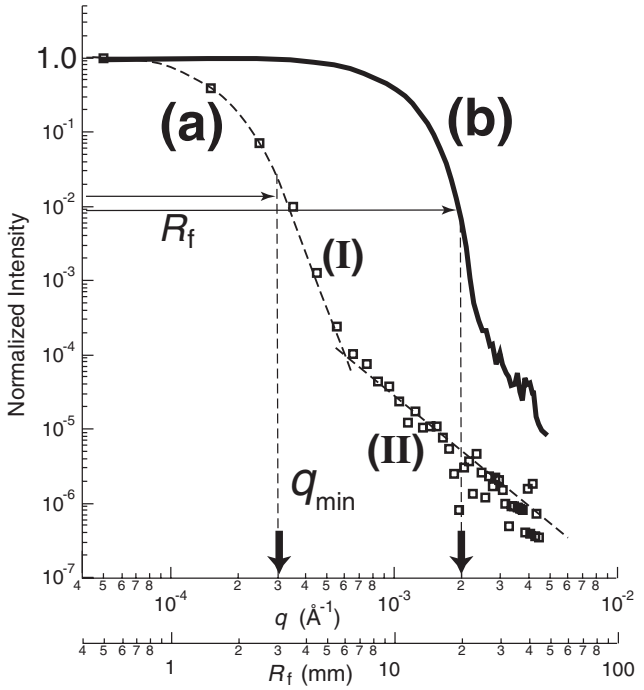

Figure 2. Direct beam profiles obtained by (a) focusing USANS with lens and (b) conventional pinhole SANS. The beam size R_f, defined as half width of the direct beam, determines minimum accessible q_{min}, as indicated by thick arrows.

length $\lambda = 6.5$ Å. The transmission of 70 individual lenses (T_{lens}) is totally about 50%.

In the vacuum flight tube, there are two position sensitive area detectors. For conventional pinhole SANS, the two-dimensional ^{3}He position sensitive main detector with a diameter of 0.58 m and about 5 mm position resolution is provided by RISΦ National laboratory in Denmark. In front of the main detector, for focusing USANS, we put high-resolution cross-wired position sensitive photomultiplier R3239 (5 inch size and 0.5 mm resolution, provided by HAMAMASTU photonics. Co. Ltd.) with ZnS/^{6}LiF scintillator in flight tube, as shown in Figure 1(a).

For a focusing USANS mode, the high-resolution area detector slides into the direct beam position, as shown in Figure 1(a). By choosing the collimation of $S_1 = 2.5$ and $S_2 = 15$ mm in (Figure 1(b)), where S is a diameter of pinhole, we can reach to $q_{min} \cong 0.0003$ Å^{-1}, which is discussed in Sec. 3-1. For a conventional pinhole SANS mode, the high-resolution area detector moves out to empty space at left bottom. By choosing the normal collimation of $S_1 = 20$ and $S_2 = 8$ mm, as shown in Figure 1(c), we can cover q-region of $0.003 < q < 0.165$ Å^{-1}, by changing detector positions ($L_S = 10$ and 2.5 m, respectively).

EXPERIMENTAL RESULTS AND DISCUSSION

Focusing Ultra-small-angle Neutron Scattering

Figure 2 shows direct beam profiles (normalized in intensity) obtained by measurement modes of (a) focusing USANS ($S_1 = 2.5$ and $S_2 = 15$ mm with lens) and (b) conventional pinhole SANS ($S_1 = 20$ and $S_2 = 8$ mm).

It is clearly recognized that profile (a) by focusing USANS is narrower (1/10) than profile (b) by conventional pinhole SANS. For profile (a), the steep drop in normalized intensity from 1 to 10^{-5} [marked by (I) in Figure 2] is attributed to chromatic aberration as a result of the wavelength distribution ($\Delta\lambda/\lambda$).[1] At intensity lower than 10^{-5}, the profiles (a) starts to fall gradually as q^{-3} [as marked by (II) in Figure 2]. This fall (II) can be attributed to parasitic scattering of the beam by slit, air, aluminum windows or imperfections of the lens. As we discussed in ref 15, this gradual decay (II) is crucial in limiting q_{min}, especially for differential scattering cross section $d\Sigma/d\Omega < 100$ cm^{-1}. To show ability of focusing optics for USANS, test

measurements on a standard sample (using polymer film with macrophase separation) has been done and reported in the ref 15.

We define a beam size R_f as a half width of the steep upturn, as defined in Figure 2. For focusing and conventional pinhole collimations, $R_f \cong 3$ and 30 mm, respectively. According to the established principle of small-angle scattering,[16] q_{min} is given by

$$q_{min} = 2\pi R_f/(\lambda L_S). \quad (1)$$

Therefore, we obtain $q_{min} \cong 0.0003\,\text{Å}^{-1}$ for a focusing USANS collimation ($R_f = 3$ mm, $L_S = 9.6$ m and $\lambda = 6.5$ Å), whereas $q_{min} \cong 0.002\,\text{Å}^{-1}$ for a conventional pinhole SANS collimation ($R_f = 30$ mm, $L_S =$ 9.6 m and $\lambda = 6.5$ Å).

A brute force method, simply narrowing beam ($S_1 = 2$ mm and $S_2 = 1$ mm), also provides narrow beam size ($R_f \cong 3$ mm). However, we expect a large intensity gain for focusing USANS, as compared to a brute force method. The gain factor g is simply given by a ratio of pinhole sizes between two collimations, considering T_{lens}, ($g = [(S_1S_2)_f{}^2 T_{lens}]/(S_1S_2)_p{}^2)$). We estimated $g \cong 175$ with $T_{lens} = 0.5$.

Time-resolved Observation on Living Polymerization Solution

First, by conventional pinhole SANS, covering q-region ($0.003 < q < 0.1\,\text{Å}^{-1}$), we examined time-evolution of microdomain structure in the reaction vessel for reaction process (II). Figure 3 shows SANS q-profiles obtained at different polymerization time after starting reaction process (II) (at 5, 75, 153, and 350 min), in which scattering intensity is relatively shifted to clearly show their q-dependences. At 5 min, we obtained SANS due to homogeneous solution, *i.e.*, PMMA or PMMA-*b*-PS chains growing by radical polymerization are dissolved in a matrix of unreacted styrene-d_8. Note that styrene-d_8 behaves as a good solvent for PMMA, PS, and PMMA-*b*-PS. At 75 min, scattering maxima, due to interparticle interference, appear at q-positions as indicated by arrows. The relative ratio of peak positions is 1/2, indicating that a lamellar microdomain appears in polymerization solution. As the polymerization time proceeds to 153 min, the first scattering maximum shifts to lower q and the relative ratio of peak positions changes as $1/3^{1/2}$, indicating a cylindrical microdomain, in which PMMA cores are dispersed in a matrix of PS corona chains and styrene-d_8. At 350 min, we cannot observe the scattering maxima due to microdomains, because these maxima appear in dark shadow region of Figure 3, which is beyond q_{min} by conventional pinhole SANS. According to focusing USANS, which is discussed next, the SANS q-profile at 350 min is due to a spherical microdomain.

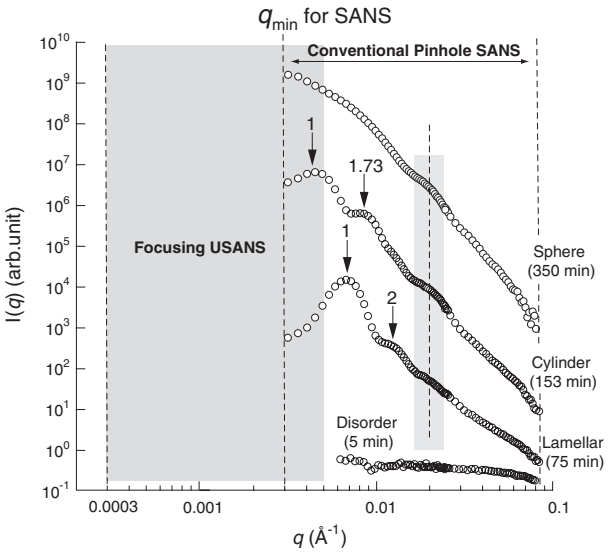

Figure 3. Time-evolution of small-angle neutron scattering profiles at 5, 75, 153, and 350 min obtained in reaction process (II). Conventional SANS reaches to $q_{min} = 0.003\,\text{Å}^{-1}$, whereas focusing USANS covers the q-region colored by gray.

All scattering q-profiles, shown in Figure 3, exhibit a broad scattering maximum due to intraparticle scattering, as indicated by a broken line at $q = 0.02\,\text{Å}^{-1}$. It should be stressed that q-position of scattering maximum due to intraparticle interference of PMMA domain does not change in the course of polymerization. This is mainly because molecular weight of PMMA block chains is constant and only PS block chains are growing by living radical polymerization during reaction process (II). In general, the q-position of intrapaticle scattering depends not only on molecular weight but also on its morphology. However, q-shift due to the morphological change is negligibly small, as compared to the instrumental q-resolution.

In order to investigate USANS q-region, indicated by a dark shadow region in Figure 3, we performed focusing USANS measurements by using incident beam narrowly collimated by focusing as shown in Figure 2. Figure 4 shows *in situ* and time-resolved focusing USANS profiles, observing after 100 min in reaction process (II). We stress that a time-slice of individual measurements is 10 min ($0 < t < 450$ min) and 30 min ($450 < t < 990$ min) (t: polymerization time), monitoring over 16.5 h.

Following the time-dependence of SANS shown in Figure 3, focusing USANS detects the growth of PMMA/PS microdomains. After 100 min, the first scattering maxima due to interparticle interference appear at the edge of high-resolution detector and continuously change their intensity and q-positions toward lower q. Finally the q-position of first scattering peak (q_{max}) reaches at $q = 0.002\,\text{Å}^{-1}$. Scattering intensity at q_{max} (I_{max}) is plotted as a function time,

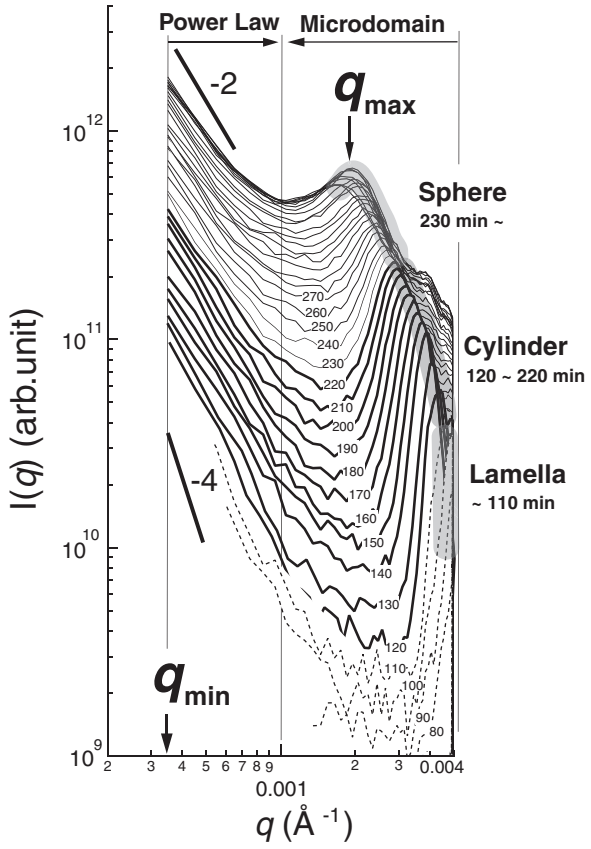

Figure 4. Time-evolution of q-profiles obtained by focusing USANS ($q_{min} = 0.00035\,A^{-1}$) in reaction process (II). The morphologies of microdomain structures change from lamella (broken lines), cylinder (thick solid lines) and sphere (thin solid lines). USANS is divided into two q-regions of power law ($q < 0.001$ Å^{-1}) and microdomain ($q > 0.001$ Å^{-1}) having scattering maximum q_{max}.

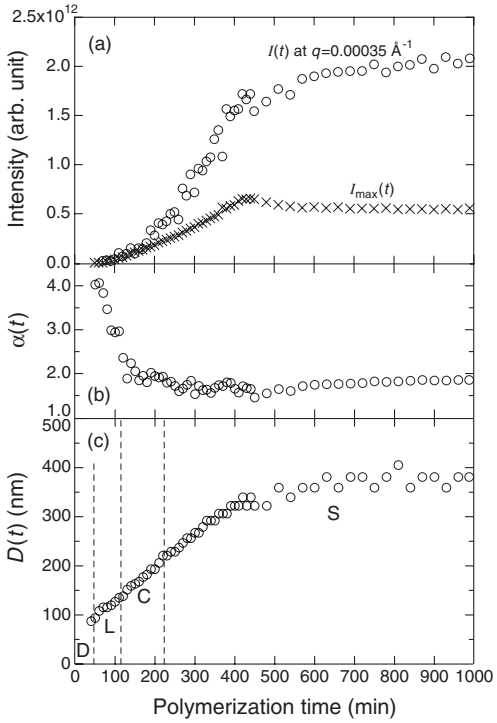

Figure 5. (a) Scattering intensities evaluated at q_{min} (open circles) and at q_{max} of microdomain structures (crosses), (b) scattering power $\alpha(t)$, evaluated from USANS q-region ($q < 0.001$ Å^{-1}) and (c) interdomain distance $D(t)$ ($= 2\pi/q_{max}$), plotted as a function of polymerization time.

as shown in Figure 5(a). I_{max} monotonically increases until 420 min and then slightly decreases. In Figure 5(c), interdomain distance $D(t)$ ($= 2\pi/q_{max}$) was determined as a function of polymerization time. $D(t)$ increases linearly with polymerization time and becomes constant after 450 min, when a spherical microdomain appears in the reaction solution.

In the beginning of reaction process (II), polymerization solution becomes turbid, which was clearly recognized by eyes. This is because macroscopic inhomogeneity between constituents appears (PMMA-*b*-PS and PS homopolymer) in the course of living polymerization. Simultaneously, strong upturn of scattering intensity appears after 100 min at lower-q region ($q < 0.001$ Å^{-1}). The scattering intensity at $q = 0.00035$ Å^{-1}, nearly at q_{min}, is also plotted in Figure 5(a). The upturn of scattering was evaluated according to a power law scattering behavior ($\sim q^{-\alpha}$), shown in Figure 5(b). In the beginning of polymerization when a lamellar microdomain appears, α is nearly equal to 4, which is a so-called Porod law[17] due to sharp interface. Then, α gradually decreases with proceeding polymerization between 120 and 220 min. When a cylindrical microdomain appears, α changes from 3 to 2. After 220 min, when a spherical microdomain appears, α remains about 2. According to gel permeation chromatography (GPC) measurement, molecular weight of PMMA-*b*-PS after finishing polymerization $M_n = 349{,}000$ and $M_w/M_n = 2.1$, respectively.

To describe q-behavior of the scattering profiles obtained by focusing USANS, we employ a scattering function given by sum of two contributions, *i.e.*, power low scattering $Aq^{-\alpha}$ and scattering function from microdomains $\Im(q)$, as follows,

$$I(q) = K\Delta b^2[Aq^{-\alpha} + \Im(q)], \qquad (2)$$

where K and Δb are an instrument constant and scattering contrast, respectively. $\Im(q)$ is composed of lattice $S(q)$ and form factors $f(q)^2$ for the microdomain ($\Im(q) = S(q)f(q)^2$). The first term of $Aq^{-\alpha}$ appears dominantly at $q < 0.001$ Å^{-1}, whereas the second term from microdomain structure appears dominantly at $q > 0.001$ Å^{-1}.

Figure 6(a) schematically describes time-evolution of micro- and macrodomains in the reaction vessel. After starting reaction process (II), macrophase separation occurs between PMMA-*b*-PS and PS homo-

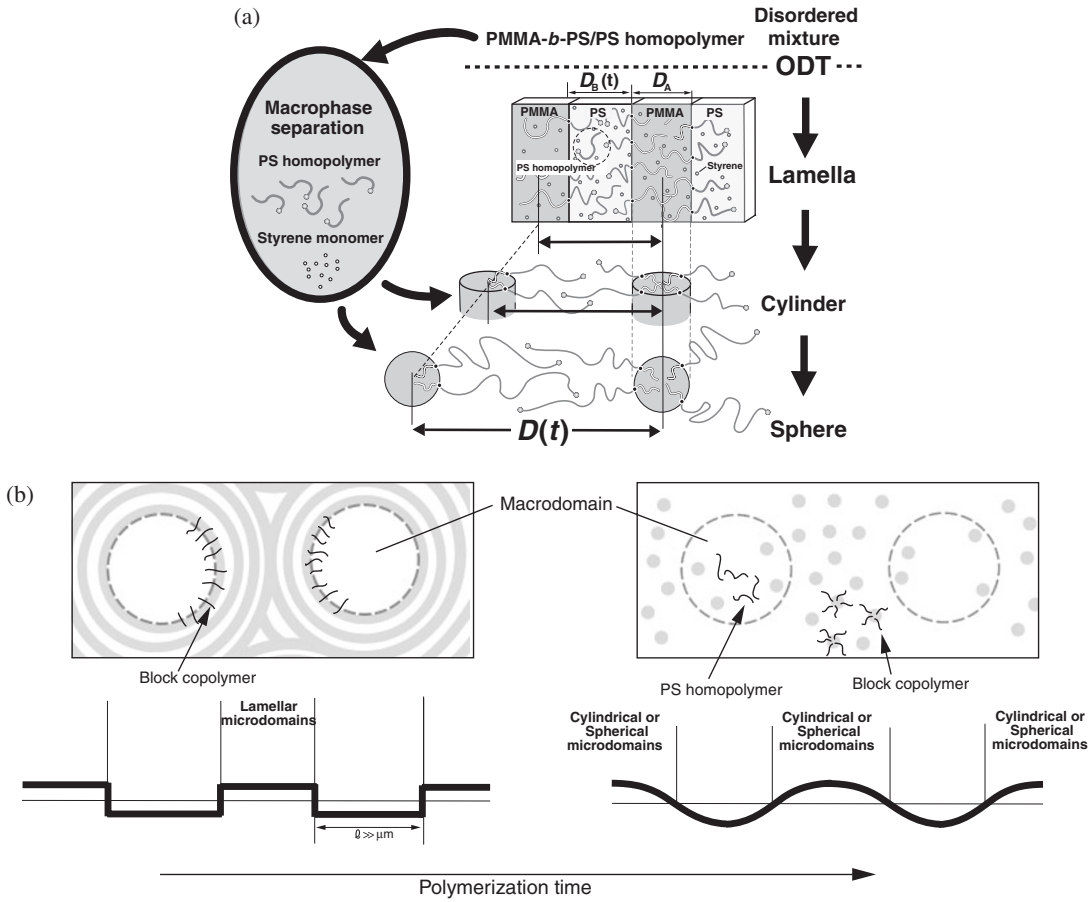

Figure 6. Schematic diagram, showing macrophase separation between PMMA-*b*-PS and PS homopolymer, order-disorder transition of PMMA-*b*-PS, order-order transitions of microdomain structure, occurring as the polymerization time proceeds and interdomain distance $D(t)$ ($= D_A + D_B(t)$) increases. (b) Spatial distribution in scattering length in length scales of micrometer, changing as the polymerization time proceeds.

polymer, which was confirmed by eyes. As the polymerization proceeds, ϕ_P and N increases by living radical polymerization. When $\phi_P \chi N$ exceeds a critical value for microphase separation, order-disorder transition (ODT) occurs and lamellar microdomain appears. It should be stressed that χ, Flory interaction parameter, is constant during living polymerization solution, because the temperature was kept at 130 °C.

D, interdomain distance shown in Figure 5(c), changes as a function of polymerization time due to domain growth of PS microdomain, given as follows,

$$D(t) = D_A + D_B(t), \tag{2}$$

where subscripts A and B denote PMMA and PS block chains. Note that D_A remains constant because PMMA block chains do not grow, which was confirmed by SANS. In a macrodomain rich-in PS homopolymer, PS homopolymer may be swollen by styrene monomers. As the living radical polymerization proceeds, styrene monomers diffuse into PS microdomain and the PS block chain grows *via* RAFT living radical polymerization. Simultaneously PS homopolymer, in the macrodomains rich-in PS homopolymer, might diffuse into the PS microdomains. As a result of two contributions, *i.e.*, growth of PS block chains and penetration of PS homopolymer into the PS microdomain, $D_B(t)$ increases as a function of polymerization time. As asymmetry between D_A and D_B increases by living polymerization, order-order transition in microdomain morphology (OOT) from lamella to cylinder, and from cylinder to sphere occur as illustrated in Figure 6(a).

α, evaluated at $q < 0.001\,\text{Å}^{-1}$, changes coupled with OOT in reaction process (II). Note that microdomains appear in the macrodomain rich-in PMMA-*b*-PS. α close to 4, we found in the beginning of reaction process (II), is a so-called Porod law due to sharp interface. Lamellar microdomains at the boundary result in the sharp interface (schematically shown in Figure 6(b)). We found large decrease in α when a cylindrical or spherical microdomain appears. α, close to 2, might be attributed to inhomogeneity of spatial distribution of cylindrical or spherical microdomains. The boundary between two macrodomains rich-in PS homopolymer and PMMA-*b*-PS becomes broader (Figure 6(b)). This is because PS or styrene-d_8 mono-

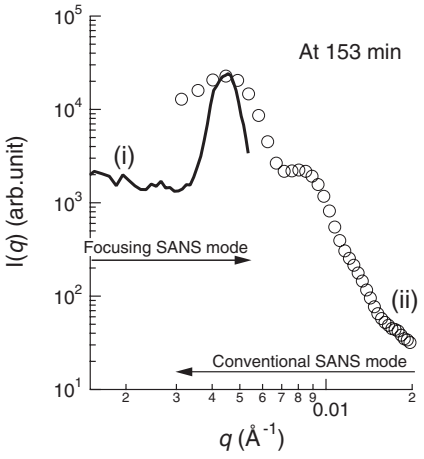

Figure 7. The 1st scattering maximum of a cylindrical microdomain structure (at 153 min in reaction process (II)), observed by (i) focusing USANS (solid line) and (ii) conventional pinhole SANS (open circles).

mers diffuse into the macrodomain rich-in PMMA-*b*-PS.

Figure 7 compares the scattering maxima of lamellar microdomain at 153 min observed by (i) focusing collimation with narrowly collimated incident beam (profile (a) in Figure 2) and (ii) pinhole collimation (profile (b) in Figure 2). The focusing collimation is advantageous to improve q-resolution ($\Delta q/q$) in the conventional q-region around $q = 0.003$ Å^{-1}.[1] The width of first scattering maximum observed by focusing collimation is much narrower than that by the conventional pinhole collimation. This is because $\Delta q/q$ by focusing collimation is dominated by $\Delta\lambda/\lambda$ ($= 0.13$) and free from R_f in the q-region at $q = 0.003$ Å^{-1}, whereas that by conventional pinhole collimation is further affected by R_f, as well as $\Delta\lambda/\lambda$.

CONCLUSION

We performed *in situ* and time-resolved focusing USANS measurements on living radical RAFT polymerization of PMMA-*b*-PS in the reaction process (II), where the PS block chain is growing from the end of PMMA block chain. Focusing USANS, which is realized by a biconcave refractive lens and high resolution cross-wired photo-multiplier with ZnS/^{6}LiF scintillater, plays an important role to determine the microdomain and macrodomain structures, appearing in the polymerization solution. The power law q-behavior of USANS at $q < 0.001$ Å^{-1}, originating from the boundary structures of the macrodomain, is affected by the morphologies of PMMA/PS microdomains, giving a rise of SANS at $q > 0.001$ Å^{-1}.

REFERENCES

1. S. Koizumi, H. Iwase, J. Suzuki, T. Oku, R. Motokawa, H. Sasao, H. Tanaka, D. Yamaguchi, H. M. Shimizu, and T. Hashimoto, *J. Appl. Crystallogr.*, **40**, s474 (2007).
2. S.-M. Choi, J. G. Barker, C. J. Glinka, Y. T. Cheng, and P. L. Gammel, *J. Appl. Crystallogr.*, **33**, 793 (2000).
3. U. Bonse and M. Hart, *Appl. Phys. Lett.*, **7**, 238 (1965).
4. J. Chiefari, Y. K. Ercole, C. J. Glinka, F. Krstina, J. Jeffery, T. P. T. Le, R. T. A. Mayadunne, G. F. Meijs, C. L. Moad, G. Moad, E. Rizzardo, and S. H. Thang, *Macromolecules*, **31**, 5559 (1998).
5. Y. K. Chong, J. Krstina, T. P. T. Le, G. Moad, A. Postma, E. Rizzardo, and S. H. Thang, *Macromolecules*, **36**, 2256 (2003).
6. E. Helfand and Y. J. Tagami, *J. Chem. Phys.*, **56**, 3592 (1972).
7. T. Hashimoto, M. Shibayama, and H. Kawai, *Macromolecules*, **16**, 1093 (1983).
8. P. G. de Gennes, in "Scaling Concepts in Polymer Physics," Cornell University Press, N.Y., Ithaca, 1979.
9. I. W. Hamley, in "The Physics of Block Copolymers," Oxford University Press, New York, 1998.
10. K. Yamauchi, H. Hasegawa, T. Hashimoto, H. Tanaka, R. Motokawa, and S. Koizumi, *Macromolecules*, **39**, 4531 (2006).
11. R. Motokawa, S. Koizumi, Y. Zhao, and T. Hashimoto, *J. Appl. Crystallogr.*, **40**, s645 (2007).
12. F. Q. John, R. Ezio, and T. P. Davis, *Chem. Commun.*, 1044 (2001).
13. K. S. Khuong, W. H. Jones, W. A. Pryor, and K. N. Houk, *J. Am. Chem. Soc.*, **127**, 1265 (2005).
14. L. Rosta, *Physica B*, **156–157**, 615 (1989).
15. S. Koizumi, H. Iwase, J. Suzuki, T. Oku, R. Motokawa, H. Sasao, H. Tanaka, D. Yamaguchi, H. M. Shimizu, and T. Hashimoto, *Physica B*, **385–386**, 1000 (2006).
16. A. Guinier and G. Fournet, in "Small-Angle Neutron Scattering of X-rays," John Wiley and Sons, Inc., New York, 1955.
17. W. J. Ruland, *J. Appl. Crystallogr.*, **4**, 70 (1971).